Applied Surface Science 695 (2025) 162893

Contents lists available at ScienceDirect

Applied Surface Science

journal homepage: www.elsevier.com/locate/apsusc

Full Length Article

Insight into charge carrier dynamics and interface design of {0 0 1} TiO_2 coupled with $TiOF_2$ for photocatalytic degradation of contaminants of emerging concern

Marta Kowalkińska [a,*], Nicolas Keller [b], Fernando Fresno [c], Christophe Colbeau-Justin [d], Anna Zielińska-Jurek [a,*]

[a] Department of Process Engineering and Chemical Technology, Faculty of Chemistry, Gdansk University of Technology, 80-233 Gdansk, Poland
[b] Institut de Chimie et Procédés pour l'Energie, l'Environnement et la Santé (ICPEES) CNRS/University of Strasbourg, 25 rue Becquerel, 67087 Strasbourg, France
[c] Instituto de Catálisis y Petroleoquímica (ICP), CSIC, Marie Curie 2, 28049 Madrid, Spain
[d] ICP, Institut de Chimie Physique, CNRS UMR 8000, Université Paris-Saclay, Bâtiment 349, CEDEX, 91405 Orsay, France

ARTICLE INFO

Keywords:
TiO_2/$TiOF_2$
Titanium oxyfluoride
Hydroxyl radicals generation
Photocatalyst
TRMC

ABSTRACT

Herein, the role of titanium oxyfluoride ($TiOF_2$) on the charge carriers generation and electron transport in the {0 0 1} TiO_2/$TiOF_2$ heterojunction photocatalysts was examined. Time-resolved microwave conductivity (TRMC), fluorescence lifetime spectroscopy, and DFT calculations were applied to investigate the charge carriers dynamics. These binary photocatalysts in a broad $TiOF_2$ content were further studied in photocatalytic generation of hydroxyl radicals (•OH) and degradation of several organic contaminants of emerging concern (CECs), namely 4-chlorophenol (4CP), myclobutanil (MCL) and carbamazepine (CBZ). Regardless of the CEC tested, it was found that the combination of highly-energetic {0 0 1} TiO_2 with $TiOF_2$ phase improved the photocatalytic activity compared to the pristine anatase. The presence of the $TiOF_2$ phase in the heterojunction increased the interfacial charge carriers separation and enhanced the generation of •OH radicals. Maximised photocatalytic activity and TOC reduction were observed for composites with a $TiOF_2$ content of 1.5 %–6 %, which exhibited the highest number of photogenerated charge carriers and a longer lifetime compared to those with higher $TiOF_2$ content. DFT calculations revealed high potential barriers within the $TiOF_2$ structure, which explains the optimum at a low level of $TiOF_2$ amount. Finally, high photocatalytic activity was maintained in five consecutive degradation cycles.

1. Introduction

Nowadays, with progressive industrialisation, the amount of pollutants in ground and surface water is growing. According to the European Environmental Agency (EEA) report, between 2000 and 2017, the total number of synthetic chemicals in the market was estimated at 100,000 compounds, excluding transformation products from chemicals during their life cycles [1]. Some of the commonly used cosmetic ingredients, pigments, pesticides and medicines are persistent in the environment. This leads to ongoing exposure to chemical pollution and limitation of available drinking water, which negatively affects human health and the environment. Therefore, further advances in the deployment of eco-innovations are crucial for reaching effective wastewater treatment and consequently avoiding bioaccumulation and biomagnification of contaminants of emerging concern (CECs) in the environment.

One of the promising methods that are capable of removing persistent organic pollutants and that is classified as green technology is heterogeneous photocatalysis, in which charge carriers photogenerated upon the irradiation of a semiconductor material participate in the degradation of a wide span of CECs such as e.g. phenolic compounds, pesticides and pharmaceuticals [2–4]. One of the most studied semiconductors is TiO_2, which has been widely investigated for photocatalytic water treatment due to suitable conduction and valence band edges as well as superior photostability [5,6]. Among many efforts to improve the photocatalytic performance of TiO_2, the shape-controlled strategies have been the focus of much effort to obtain highly energetic surfaces as the photocatalytic activity critically depends on the

* Corresponding authors.
E-mail addresses: marta.kowalkinska@pg.edu.pl (M. Kowalkińska), annjurek@pg.edu.pl (A. Zielińska-Jurek).

https://doi.org/10.1016/j.apsusc.2025.162893
Received 29 November 2024; Received in revised form 15 February 2025; Accepted 4 March 2025
Available online 5 March 2025

crystal facets exposition [7–9]. Recently, anatase {0 0 1} crystal facets have been extensively studied since the research presented by Yang et al. proved that these facets, despite high surface energy, could be stabilized by F^- ions and formed instead of the thermodynamically stable {1 0 1} facets [10]. TiO_2 exposing a majority of {0 0 1} facets became prominent because it contains the high density of active unsaturated Ti atoms and active surface oxygen atoms, which renders numerous active sites and strong interactions with the adsorbates during the photocatalytic redox reactions [11,12]. However, our recent studies showed that anatase {0 0 1} nanosheets exhibited a low mineralisation rate of aromatic compounds, which is an important factor for CECs removal because high total organic carbon (TOC) reduction yield in the presence of the photocatalyst ensures that the substrate and any intermediate products formed during the process have been degraded [13,14].

In fluorine-rich environments during the solvothermal reaction of a Ti source, titanium oxyfluoride ($TiOF_2$), a wide bandgap semiconductor (~3.2 eV) with cubic structure, can also be formed next to anatase [15,16]. Due to the strong bonding energy of Ti—F, $TiOF_2$ is supposed to be stable at ambient conditions [17]. However, pristine $TiOF_2$ suffers from low photocatalytic activity [14,18,19], so practical applications for this material have been scarcely explored. The majority of the studies regarding titanium oxyfluoride includes phase conversion to anatase *via* calcination [16,18,20] or hydrothermal route [14,21]. The application of $TiOF_2$ in the heterojunction-based photocatalysts has not been studied yet and only a few recent studies have been reported, e.g. $TiOF_2$/g-C_3N_4 [22], Ag_3PO_4/$TiOF_2$ [23] and $TiOF_2$@$Ti_3C_2T_x$ [24]. Therefore, coupling $TiOF_2$ with facet-regulated {0 0 1} anatase may be a perfect solution for enhancing photocatalytic performance and inducing TOC reduction of aromatic pollutants, which is a serious limitation for these facets exposition. Two strong advantages support this combination: first, the comparable atomic density of states and electron binding energy between TiO_2 and $TiOF_2$ crystals lead to excellent interfacial alignment, facilitating efficient migration and separation of photogenerated electron-hole pairs [18,25]. Remarkably, the formation of {0 0 1} TiO_2/$TiOF_2$ can be performed *via* a one-step facile procedure, excluding co-catalyst deposition or interface modification with an external compound. Nevertheless, many aspects of $TiOF_2$-based photocatalysts remain unexplored, including the synthesis procedure for TiO_2/$TiOF_2$ with a controllable $TiOF_2$ content, the role of the $TiOF_2$ phase and the understanding of the photocatalytic activity enhancement [26].

Therefore, this study aims to demonstrate the promise of coupling highly energetic {0 0 1} anatase crystal facets with controlled amounts of $TiOF_2$ for the photocatalytic degradation of CECs in water under UV-A and simulated solar light. The synthesis of a span of {0 0 1} TiO_2/$TiOF_2$ binary photocatalysts in various $TiOF_2$ contents was performed under pronounced steric hindrance conditions, in order to study the mechanism of $TiOF_2$ formation. The activity of these binary photocatalysts was assessed in the degradation and mineralisation of several persistent organic pollutants aiming to expand the scope of the study, namely 4-chlorophenol (4CP), carbamazepine (CBZ) and myclobutanil (MCL). 4CP is a compound widely used in the textile industry, whereas the anticonvulsant drug CBZ has been proposed as an anthropogenic marker of water quality [27–29]. The degradation of the triazole pesticide MCL has been still rarely reported in the literature compared to that of other organic pollutants so this compound was also selected for investigation [30]. Moreover, the photocatalytic generation of hydroxyl radicals (•OH) was monitored and discussed. The behaviour of the photogenerated charge carriers and the electronic structure of {0 0 1} TiO_2/$TiOF_2$ were extensively studied by fluorescence lifetime measurements, time-resolved microwave conductivity (TRMC) analysis and density functional theory (DFT) calculations. Finally, reusability tests were performed for the most efficient photocatalyst.

2. Results and discussion

The synthesis protocol and characterisation methods applied in this work can be found in Supplementary Materials.

2.1. Material characterisation

Two distinct phases, namely anatase TiO_2 (reference ICDD no. 01-070-8505) and titanium oxyfluoride $TiOF_2$ (no. 01-077-0132), were noticed in the photocatalysts, as presented in Fig. 1a. No additional peaks corresponding to other compounds were detected. The detailed structural parameters of the photocatalyst series are presented in Table 1. Based on the XRD analysis, the predominant role of the synthesis time was confirmed. With the increasing time of solvothermal synthesis, the content of anatase rises and the (101) peak at $2\theta = 25.5°$ becomes more distinct. Simultaneously, the content of titanium oxyfluoride decreased with increasing the reaction time. This can be explained by the progressive transformation of $TiOF_2$ into TiO_2. For samples synthesised over times exceeding 16 h, *ie.* S-16 h and S-24 h, the main (100) peak at $2\theta = 23.7°$ related to $TiOF_2$ has completely vanished, and only pure anatase can be observed.

In addition to the phase composition, the synthesis time mainly influences three structural parameters, namely the mean anatase crystallite size, the amorphous phase content and the specific surface area. The relationship between these parameters and the time of solvothermal synthesis is presented in Fig. S1 in Supplementary Materials. Globally, the longer the synthesis time, the larger the mean anatase crystallite size, so pure anatase samples (S-16 h and S-24 h) exhibit larger mean crystallite sizes than the binary TiO_2/$TiOF_2$ samples. Also, the amorphous phase content increased during the first few hours of the solvothermal reaction, reaching a maximum content for 6 h of synthesis, before dropping down to reach a minimum value for S-24 h when decreasing the $TiOF_2$ content. This effect can be explained by the fact that freshly synthesised TiO_2 is not fully crystallised and contains a high fraction of the amorphous phase. During the solvothermal reaction, progressive crystallisation of the anatase structure occurs, resulting in the decrease of the amorphous phase contribution. Additionally, the specific surface area of the samples followed a volcano-like trend within the 80–100 m^2/g range with the increase in the synthesis time, the highest values being for S-8 h and S-10 h. Those features correlate well with the simultaneous occurrence of both $TiOF_2 \rightarrow TiO_2$ phase transformation and the progressive crystallisation process of the pure anatase phase. By contrast, a low specific surface area of 5 m^2/g was observed for pure $TiOF_2$.

Fig. 1b compares the FTIR spectra of $TiOF_2$, {0 0 1} TiO_2 and {0 0 1} TiO_2/$TiOF_2$ with different phase compositions. The stretching and bending vibrations due to adsorption of H_2O and the Ti—OH groups are found at 3100–3600 cm^{-1} and 1630 cm^{-1}, respectively [5]. Bands located at 539 cm^{-1} and 455 cm^{-1} can be attributed to Ti—O or Ti—O—Ti vibrations. Strong absorption peaks centered at 992 cm^{-1} are ascribed to Ti—F bonds [31]. Remarkably, the intensity of this band is dependent on the $TiOF_2$ content – for pristine titanium oxyfluoride it is the most distinct and decreases with increasing anatase content. Finally, for samples prepared with a solvothermal synthesis time exceeding 8 h, this band cannot be distinguished. This observation can be strictly correlated with the progressive tranformation from $TiOF_2$ to TiO_2.

SEM images in Fig. 2a revealed that the pristine $TiOF_2$ titanium oxyfluoride phase consists of irregular cubes. With increasing the synthesis time, the formation of two-dimensional anatase nanoparticles is observed, which resulted from the presence of F^- ions during the solvothermal synthesis. These ions stabilise the highly energetic {0 0 1} facets and promote growth in the *hk* direction [13,32]. However, differences between the anatase nanosheets can be noted, as binary

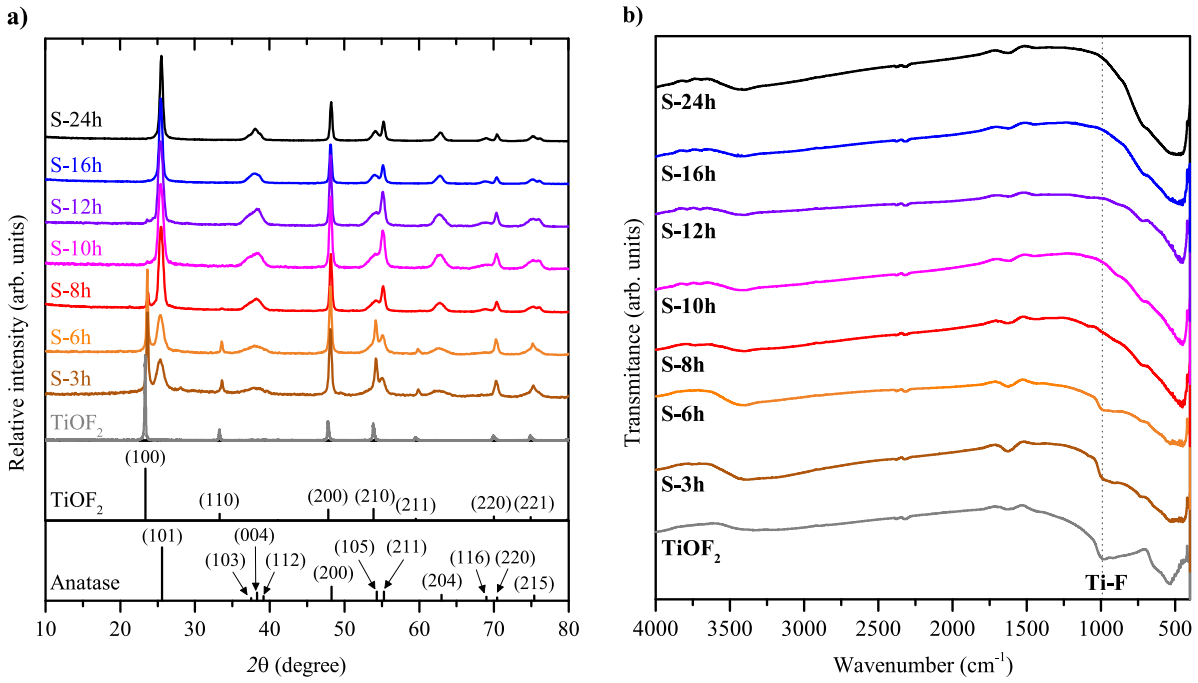

Fig. 1. a) XRD patterns and b) FTIR spectra of the {0 0 1} TiO_2/$TiOF_2$ series samples.

Table 1
Characterisation of the photocatalysts using XRD, BET and XPS analyses.

Sample name	Phase composition (%)		Mean anatase crystallite size (nm) *	Amorphous phase content (%)	Surface area (m^2/g)	Surface Ti/F ratio
	TiO_2	$TiOF_2$				
$TiOF_2$	-	100	43	-	5	0.5
S-3h	56	44	8	42	79	1.1
S-6h	74	26	9	60	78	1.2
S-8h	94	6	13	54	99	2.5
S-10h	98.5	1.5	11	54	102	3.7
S-12h	>99	<1	12	47	82	n.c.
S-16h	100	-	17	36	84	n.c.
S-24h	100	-	19	21	78	4.9

*For TiO_2-containing samples, the mean anatase crystallite size was calculated based on the (101) peak. For $TiOF_2$, the mean crystallite size was calculated based on the (100) peak. The mean crystallite size for anatase, defined as the average size of the coherent diffracting domains, remains an estimate as it was determined from the Scherrer equation with the usual assumption of spherical crystallites.
n.c.: non calculated.

samples S-3 h, S-8 h and S-12 h displayed thicker and wider TiO_2 nanostructures than in the single-phase counterpart (sample S-24 h). In the {0 0 1} TiO_2/$TiOF_2$ samples S-3 h, S-8 h and S-12 h, the irregular cubes assigned to the $TiOF_2$ titanium oxyfluoride phase displayed a larger size than the thick nanosheets. These bulk particles were not noticed in the S-12 h sample, as the $TiOF_2$ content remains by far much lower (<1 %) than for samples synthesised with shorter reaction times.

The synthesis time had an impact either on the TiO_2 content or on the morphology changes. Based on SEM and XRD results, the {0 0 1} TiO_2/$TiOF_2$ formation under solvothermal conditions with n-hexanol as a solvent and its transformation to pure anatase is proposed to rely on the following mechanism (Eqs. 1–3) [15,33,34]:

$$2\ \text{R-OH} \rightarrow \text{R-O-R} + H_2O, \quad (1)$$

$$(\text{R-O})_n TiF_{4-n} + n\ H_2O \rightarrow TiOF_2 + n\ \text{R-OH} + n\ \text{HF}, \quad (2)$$

$$TiOF_2 + H_2O \rightarrow TiO_2 + 2\ \text{HF}. \quad (3)$$

Generally, in the presence of alcohols and HF, the Ti precursor undergoes alcoholysis and forms $(\text{R-O})_n TiF_{4-n}$ complex. However, for further transformation to titanium oxyfluoride Eq. (2), H_2O molecules are needed, which amount is limited in solvothermal conditions. Therefore, alcohol condensation Eq. (1) is probably due to high temperature and increased pressure. The nucleation is slow due to the use of long-chain alcohol as a solvent and, in consequence, steric hindrance [13]. H_2O also participates in the hydrolysis of $TiOF_2$ to anatase Eq. (3). However, it is well-known that the subsequent {0 0 1} TiO_2 growth is a result of HF-mediated dissolution-recrystallisation processes, in which the Ti species are reversibly transferred between its solid oxide form and dissolved ion, preferably coordinated with 6 ligands in the form of bipyramid. In addition, an alcohol exchange with halide ligands is possible under solvothermal conditions [20,35]. The scheme of these transformations is presented in Fig. 2b. The more dissolution-recrystallisation processes occur, the more stable and defect-free TiO_2 structure is formed, which explains the relatively low amorphous phase content in the S-24 h sample. Finally, longer durations of solvothermal synthesis provide more H_2O to the reaction environment so that when the Ti precursor is fully transformed to anatase, this new structure is surrounded by F^- ions and water molecules. While the {0 0 1} facets can be stabilised mainly by fluoride ions, H_2O can promote the formation of low-energetic crystal facets like {1 0 0} [36]. This is a probable reason for the formation of wider nanosheets in the pure anatase S-24 h sample compared to the binary photocatalysts. The proposed mechanism of the

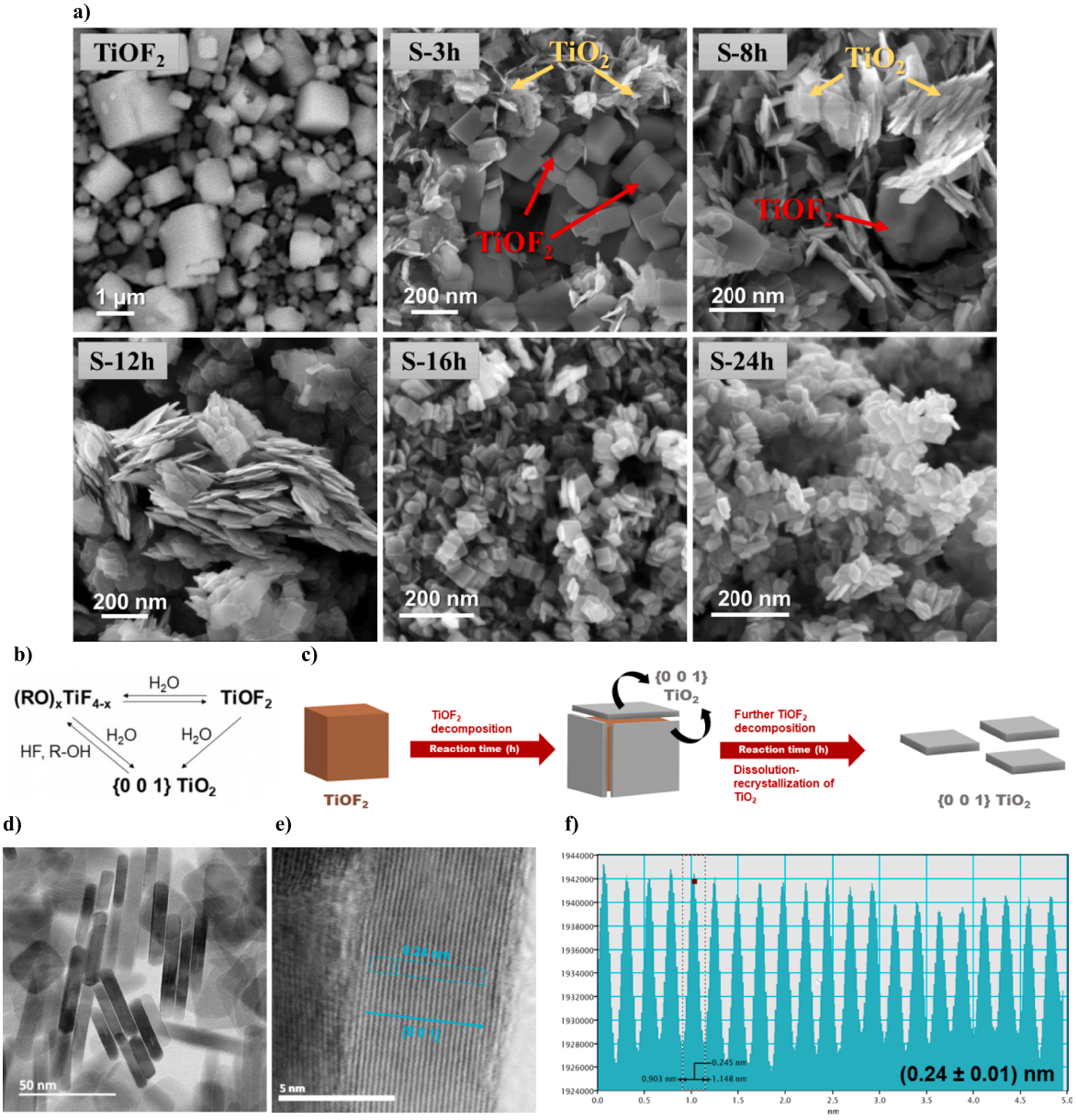

Fig. 2. a) SEM images of the $TiO_2/TiOF_2$ series samples, for samples S-3 h and S-8 h, $TiOF_2$ and anatase TiO_2 phases are marked with red and yellow arrows, respectively. b) Transformation of Ti species under solvothermal conditions and c) proposed mechanism of the morphology transformation from $TiOF_2$ cubes to {0 0 1} TiO_2. d) TEM and e) HRTEM image of the {0 0 1} TiO_2 (sample S-16 h) in bright-field mode, f) line profile image.

morphological changes is schematically presented in Fig. 2c.

The formation of {0 0 1} facets in anatase nanosheets was confirmed by transmission electron microscopy (TEM). The TEM images of S-16 h presented in Fig. 2d revealed a well-defined sheet-shaped structure. As shown in HRTEM images (Fig. 2e) and corresponding line profile image (Fig. 2f), the lattice spacing parallel to the front of the nanosheets was calculated to be ~0.24 nm, which is a direct confirmation that the exposed top and bottom facets belong to {0 0 1}, because these planes are arranged to [0 0 1] direction [37].

DRS analysis performed on the $TiO_2/TiOF_2$ series within the 200–800 nm range (Fig. 3a) exhibited the absorption band and edge characteristic for both anatase and titanium oxyfluoride phases [14,38]. Pure $TiOF_2$ is grey with a small band above 380 nm, which further vanishes during TiO_2 formation. The derived Tauc plot evidenced that the bandgap energy of the samples was not significantly influenced by the phase composition and the morphology changes (Fig. S2 in Supplementary Materials).

Furthermore, ζ potential as a function of pH was studied to investigate the interaction between the photocatalyst surface and the pollutant. Based on the zeta potential analysis presented in Fig. S3 in Supplementary Materials, the isoelectric point (IEP), which is defined as the pH where the electrophoretic mobility changes from positive to negative, was determined. For the samples S-24 h (pure anatase) and S-10 h ($TiO_2/TiOF_2$), the IEP values were 5.7 and 5.5, respectively. Compared to the literature value of the isoelectric point for TiO_2 (6.2) [39,40], a slight shift towards acidic conditions can be observed. This effect can be explained by differences in the surface atom arrangement due to the exposition of {0 0 1} facets stabilised by fluorine ions. The presence of F^- and the unique morphology obtained influence the rates of surface hydroxylation and protonation compared to bulk TiO_2 [41]. Moreover, $IEP_{S\text{-}10h}$ is slightly lower than $IEP_{S\text{-}24h}$, which is probably a result of the presence of the titanium oxyfluoride phase in the photocatalyst, which causes different electronic distribution on the surface compared to pure {0 0 1} anatase nanocrystals.

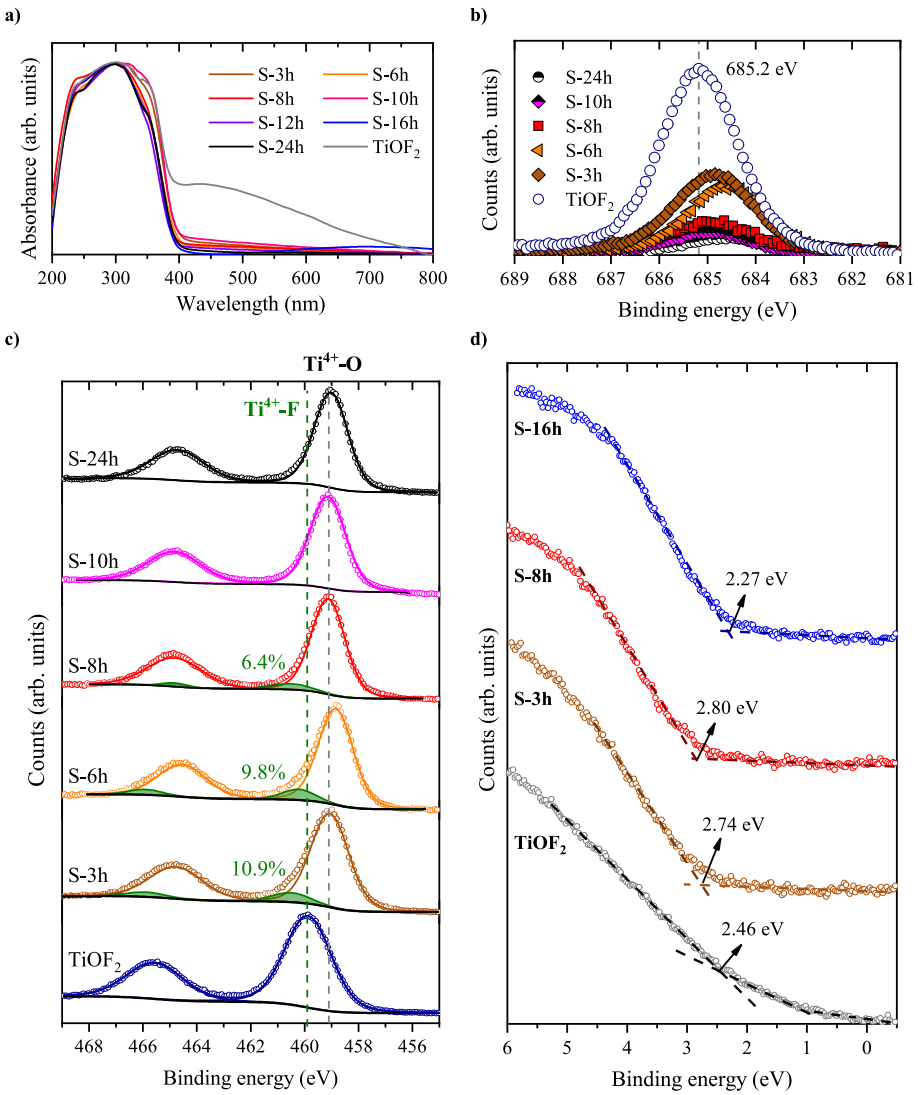

Fig. 3. a) DR/UV–vis absorption spectra of the photocatalysts, b) F1s and c) Ti2p orbital XPS spectra recorded on selected samples from the $TiO_2/TiOF_2$ series, d) VB-XPS spectra of selected photocatalysts.

The photocatalyst surface was also studied using X-ray photoelectron spectroscopy (XPS). The XPS spectra at F1s and Ti2p core orbital regions recorded on the binary $TiO_2/TiOF_2$ samples with different $TiOF_2$ contents and both pure $TiOF_2$ and anatase (S-24 h) samples are depicted in Fig. 3a-b. The survey scans of all the samples are shown in Fig. S4 in Supplementary Materials. The spectra recorded on the pure titanium oxyfluoride material showed a characteristic symmetrical contribution at 685.2 eV ascribed to F^- ions (F1s orbital), and a well-defined Ti^{4+} Ti $2p_{3/2}$-Ti $2p_{1/2}$ doublet at 459.9 eV and 465.6 eV with a spin–orbit coupling constant of 5.7 eV (Ti2p orbital) [13,15]. The bulk transformation of the $TiOF_2$ phase into TiO_2 with increasing the synthesis duration is accompanied by a surface change, and the Ti2p orbital spectra recorded on binary $TiO_2/TiOF_2$ samples were characterised by the presence of two well-defined Ti^{4+} doublets, with the contribution of Ti^{4+}—O bonds at ca. 459.1 eV and 464.8 eV, and an additional doublet at higher binding energy assigned to Ti—F bonds. Contrary to the bulk ratio, the Ti^{4+}—O contribution was dominant over its Ti—F counterpart already for the short synthesis duration of 3 h. Thereby the contribution of the Ti—F species was not evidenced for synthesis durations exceeding 6 h, while simultaneously the F1s orbital signal decreased significantly when increasing the TiO_2 content with increasing the synthesis duration. Consequently, the Ti/F surface atomic ratio increased strongly with the increase in the TiO_2 content (Table 1). With the electrostatic model of chemical shifts in XPS, the higher binding energy of the Ti-F bond contribution compared to that of Ti^{4+}—O results from the higher electronegativity of fluoride *vs.* oxygen. This was also observed by Jain et al. [42], who studied the surface chemical state of TiF_4. Similar F-induced chemical shifts were observed for a span of elements [43]. However, F atoms are randomly distributed in the titanium oxyfluoride structure [44], which makes it impossible to distinguish between Ti—F and Ti—O bonds in the Ti 2p XPS spectra of pure $TiOF_2$.

Valence-band XPS spectra (VB-XPS) presented in Fig. 3d revealed the position of the valence band relative to the Fermi level. The VB edges values for pristine $TiOF_2$, {0 0 1} TiO_2 (S-16 h), S-3 h and S-8 h were 2.46 eV, 2.27 eV, 2.74 eV and 2.80 eV, respectively. S-3 h and S-8 h samples, which correspond to {0 0 1} $TiO_2/TiOF_2$ photocatalysts, exhibit a shift toward higher binding energies compared to pure compounds, which can be attributed to the modulation of Fermi level in the heterojunction.

2.2. *Photocatalytic degradation of contaminants of emerging concern*

The photocatalytic activity of the samples was studied in the degradation of organic pollutants classified as contaminants of emerging concern and differing strongly in terms of chemical functions. Firstly, the degradation of 4-chlorophenol (4CP) under UV-A light was studied.

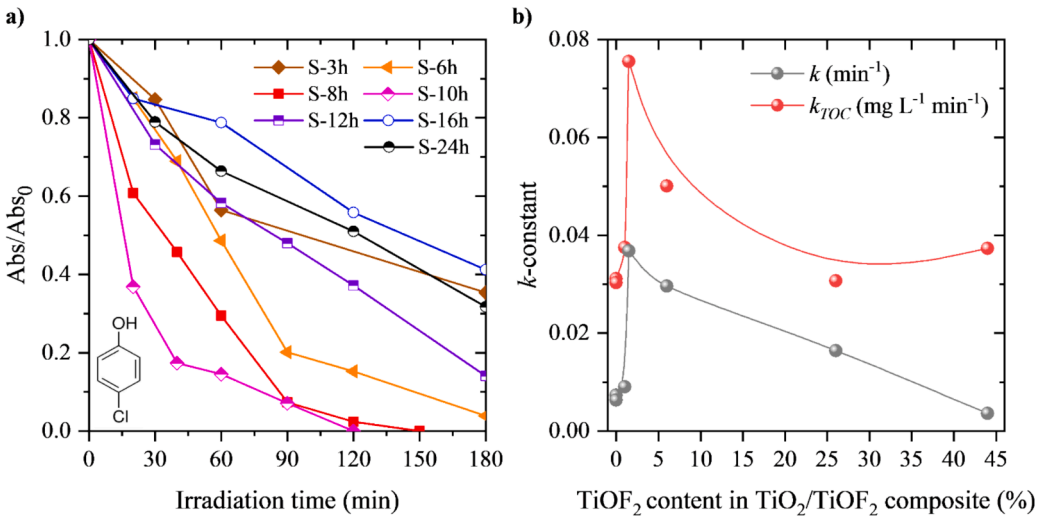

Fig. 4. a) Photocatalytic degradation of 4CP under UV-A light over $TiO_2/TiOF_2$ series, b) relationship between the *k*-constants and the $TiOF_2$ content. Process parameters: $[4CP]_0 = 20$ ppm, [cat] = 1 g/dm^3.

As presented in Fig. S5 in Supplementary Materials, pristine $TiOF_2$ revealed low photocatalytic activity, whereas Fig. 4a and Fig. S6 show that all the samples containing {0 0 1} anatase TiO_2 in the series could degrade and mineralise 4CP. The least efficient samples were S-16 h and S-24 h, which are composed of pure {0 0 1} anatase phase. Both degradation and mineralisation kinetics were accelerated when the $TiOF_2$ phase was present in the photocatalyst structure. The relationship between the $TiOF_2$ content in the heterojunction-based photocatalyst and both apparent kinetic rate constants for degradation and mineralisation evidenced a volcano-type behavior with increasing the $TiOF_2$ content (Fig. 4b). The highest apparent kinetic constants for both 4CP degradation and TOC reduction were achieved for the sample S-10 h, namely the heterojunction with a low and optimal $TiOF_2$ content of about 1.5 %. We observed that a too high titanium oxyfluoride content inhibited the photocatalytic degradation of the organic pollutant.

Based on the results of 4CP degradation, the photocatalytic activity of the samples was assessed in the degradation of CECs with more complex molecular structures, namely myclobutanil and carbamazepine. Fig. 5 depicts the evolution of the relative concentration of both pollutants for reactions conducted under pure UV-A light or simulated

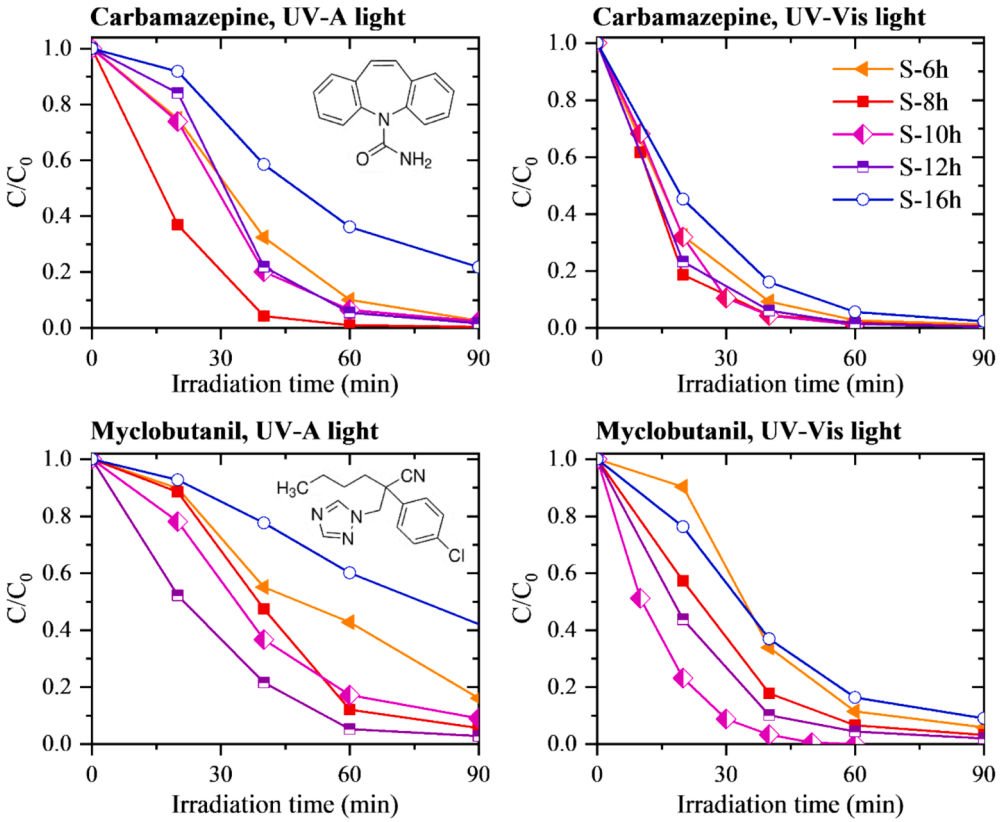

Fig. 5. Photodegradation of MCL and CBZ under UV–Vis and UV-A light using {0 0 1} TiO_2 and {0 0 1} $TiO_2/TiOF_2$. Conditions: $[CBZ]_0 = 14$ ppm, $[MCL]_0 = 20$ ppm, [cat] = 1.0 g/dm^3.

solar light, and the apparent kinetic rate constants for degradation are presented in Table S1 in Supplementary Materials. HPLC chromatograms of CBZ and MCL are shown in Fig. S7. Photolysis in the absence of photocatalysts and the linear plots of $\ln(C_0/C)$ *vs.* irradiation time are shown in Fig. S8. Pure {0 0 1} anatase samples (S-16 h and S-24 h) exhibited lower apparent kinetics than the heterojunction-based photocatalysts independently of the light source. The TOC reduction after 2 h of reaction is presented in Fig. 6. Similarly to the results with 4CP, the highest mineralisation efficiency was observed for samples with a very low $TiOF_2$ content. In the case of MCL and CBZ solutions, this corresponded to S-8 h and S-10 h samples that have a $TiOF_2$ content lower than 6 %. These samples exhibited excellent photocatalytic performance toward CECs oxidation, comparable or higher than the previous reports regarding CBZ and MCL removal (the comparison of apparent kinetic rate constants is presented in Table S2 in Supplementary Materials).

Although myclobutanil and carbamazepine are degraded, their interaction with the photocatalyst surface is different. The pH of the suspension before the photocatalytic MCL removal was 4.9. Herein, MCL occurs in the deprotonated form as pH > pKa (2.3) and therefore MCL is negatively charged in the degradation reaction conditions. The positively charged surface of the {0 0 1} $TiO_2/TiOF_2$ sample consequently favoured its interaction with the deprotonated form of the pesticide compound. After the photocatalytic process, the pH of the suspension slightly dropped down to 4.3, as a result of the release of acidic Cl^- ions during the MCL removal, which is consistent with IC chromatography analysis of the Cl^- ion concentration. By contrast, the CBZ molecule is neutral, as pH < pK_a (13.9), and therefore the electrostatic attraction with the photocatalyst surface is unlikely.

Based on Figs. 4-6, three samples – S-8 h, S-10 h and S-12 h – with a relatively low $TiOF_2$ content (below 6 %), can be distinguished as the most photocatalytically active binary systems with the highest kinetic rate constants, and for which the highest 4CP, MCL and CBZ removal, as well as the highest TOC reduction, were observed. Therefore, it can be assumed that the ability to create the $TiO_2/TiOF_2$ heterojunction is a predominant factor which affects the photocatalytic degradation of pollutants. The effect of surface fluorination also occurs, but based on our previous report [45], we can assume that the role of surface fluorination is relatively low compared to the formation of heterojunction.

However, these experiments showed that considering the degradation of MCL and CBZ, the apparent kinetic rate constant may not be correlated with the TOC reduction efficiency. For example, S-12 h exhibited *k*-constants comparable to those obtained with S-10 h and S-8 h, but the TOC conversion was significantly lower than with the aforementioned samples. This discrepancy was also observed in our previous studies about facet-engineered TiO_2 [14]. The probable reason is that the presence of titanium oxyfluoride influences the degradation pathway of the pollutant oxidation. Moreover, the interaction with the photocatalyst is different for particular CECs due to various pK_a values. Finally, the intermediate products formed during the degradation of the contaminant can have different adsorption features on the photocatalyst surface than the initial compound.

2.3. Hydroxyl radicals generation

The ability of the heterojunction photocatalysts to generate •OH radicals, which participate in the degradation and the mineralisation of the pollutant, was monitored using a coumarin fluorescence probe method. The more hydroxyl radicals are generated, the more 7-hydroxycoumarin (7-OHC) is formed by selective oxidation of the coumarin substrate. Fig. 7a shows the 7-OHC production under UV-A light obtained on selected photocatalysts, whereas the statistical analysis of coumarin fluorescence probe method is depicted in Fig. S9 in Supplementary Materials. A direct correlation is observed between the hydroxyl radicals formation (characterised by the formation of 7-OHC) and the degradation rate of CBZ and MCL, as shown in Fig. 7b. Indeed, the concentration of 7-OHC is significantly higher for the {0 0 1} $TiO_2/TiOF_2$ composites (S-8 h and S-10 h) than for pure anatase nanosheets (S-24 h). This indicates that the presence of the $TiOF_2$ phase helps in the separation of charge carriers and the enhancement of ROS generation. The high •OH generation yield obtained with the S-8 h sample is comparable to that shown by the Aeroxide© TiO_2 P25 (Degussa), as is presented in Fig. S10 in Supplementary Materials, which confirms the high photoactivity of the binary $TiO_2/TiOF_2$ photocatalysts.

Generation of •OH radicals is often the result of H_2O reaction with photogenerated holes [46,47]. Therefore, higher coumarin conversion to 7-OHC for {0 0 1} $TiO_2/TiOF_2$ can be explained by higher amount of charge carriers available to drive the reaction. This hypothesis was verified by the experiment of photocatalytic hexavalent chromium reduction, presented in Fig. S11 in Supplementary Materials. Similarly, the enhanced Cr(V) → Cr(III) conversion was observed for $TiO_2/TiOF_2$. Considering that electrons are responsible for reduction reactions, this suggests that the formation of heterojunction enhances the separation of electrons and holes.

2.4. The role of $TiOF_2$ – Charge carriers generation and separation, DFT calculations

Furthermore, to study the role of the $TiOF_2$ phase in the heterojunction at an atomic level, DFT calculations were performed. The optimised model of the (0 0 1) TiO_2/(1 0 0) $TiOF_2$ interface, along the

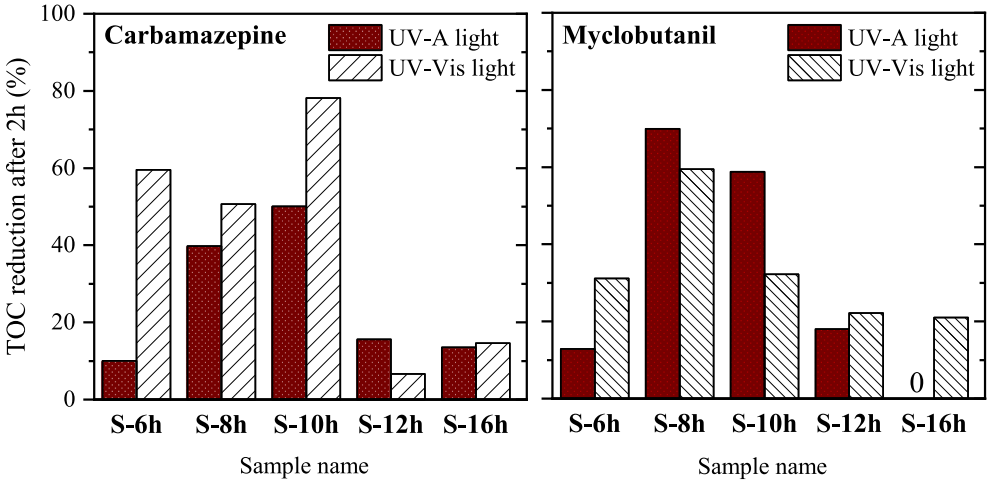

Fig. 6. TOC reduction achieved after 2 h of process under UV-A and UV–Vis light using {0 0 1} TiO_2 and {0 0 1} $TiO_2/TiOF_2$ photocatalysts.

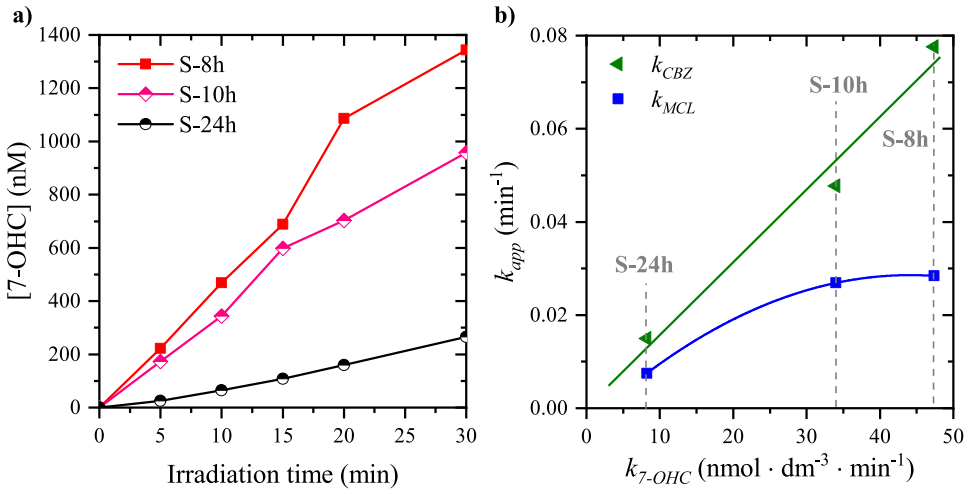

Fig. 7. a) 7-OHC generation under UV-A light, b) relationship between the apparent kinetic rate constants for CBZ and MCL degradation and the 7-OHC production derived from the slopes of Fig. 6a.

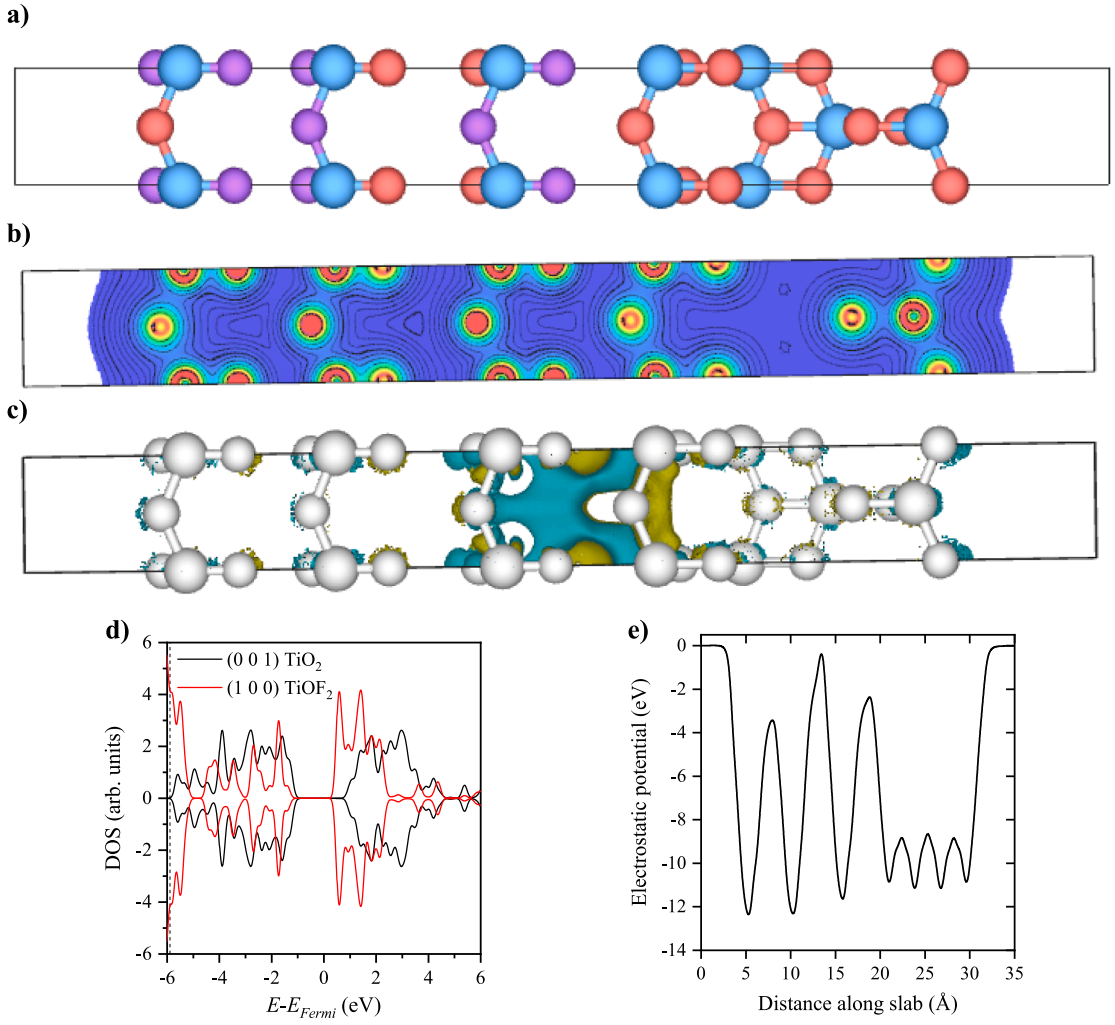

Fig. 8. a) Optimized model of the (001) TiO_2/(100) $TiOF_2$ interface, considering mutual [0 0 1] axis of both crystal structures, b) the corresponding calculated electron density distribution map, and c) charge density difference formed as the consequence of the interface formation, d) Total DOS of (0 0 1) TiO_2/(1 0 0) $TiOF_2$ interface and e) electrostatic potential plotted along the slab thickness. In panel a), Ti, O and F atoms are blue, red and purple, respectively; in panel c) element colours were omitted for better clarity.

analogical [0 0 1] axis, is presented in Fig. 8a. From the output file of SCF results (necessary for geometrical optimisation), work functions (Φ) of pristine compounds were obtained, equal to 5.87 eV and 6.76 eV for (0 0 1) TiO_2 and (1 0 0) $TiOF_2$, respectively. The $\Phi_{anatase}$ is consistent with the literature [48]. Noteworthy, the interface formation resulted in a noticeable distortion of the $TiOF_2$ geometry, with O/F atoms deviating from their cubic-phase positions and recreating lengths and angles analogical to the (0 0 1) plane of the anatase TiO_2. Following the geometry optimisation, the electronic properties of the interface were investigated based on the charge density map (Fig. 8b), and charge density difference (Fig. 8c, 3D model). As observed, overall charge density shows little difference within the model, with the most noticeable feature being preferred charge localization on the F atoms within the $TiOF_2$ structure, in agreement with the extremely high electronegativity of the fluorine. However, analysis of the charge density difference revealed further consequences of the interface formation. As presented in Fig. 8c, electron density became more affected at the interface, with a clear preference to localize charge at the interfacial F atoms and Ti-O-Ti bridge of the (0 0 1) anatase plane (dark-yellow regions in the figure). In this regard, it is expected that the formation of the $TiO_2/TiOF_2$ interface will form additional states that are especially beneficial for electron localization. To quantitatively investigate the charge change and transfer, Bader charge analysis was performed for pristine compounds and in heterojunction (Table S3 in Supplementary Materials). The positive Bader charge corresponds to electron donation, whereas negative values show the electrons gained by atoms. The highest interface effect is noticed for interfacial F atoms, which exhibited a positive value of Bader charge. These results are consistent with charge density difference plots.

The calculated density of states (DOS) of the interface between the anatase (0 0 1) surface and (1 0 0) $TiOF_2$ is presented in Fig. 8d. It can be seen that the band corresponding to $TiOF_2$ possesses lower energy than TiO_2, so the conduction band (CB) of TiO_2 will be located higher than that of $TiOF_2$. Consequently, the valence band (VB) positions also vary from each other and the VB of TiO_2 possesses higher energy than that of $TiOF_2$. Finally, plotting of the average electrostatic potential along the slab (Fig. 8e) revealed that high potential barriers exist within the $TiOF_2$ structure. Above all, this might be the reason behind the long lifetimes of the generated charge carriers observed for the $TiOF_2$, but might also contribute to its negligible photocatalytic activity, as the charge carriers might undergo trapping within the crystal structure, with the low possibility of migration and transfer after the excitation. However, as a consequence, efficient charge separation can be achieved only when $TiOF_2$ forms thin structures at the (0 0 1) TiO_2 surface. This is because further growth of the $TiOF_2$ may trap electrons at the interface and reduce their possible migration due to the high potential barriers

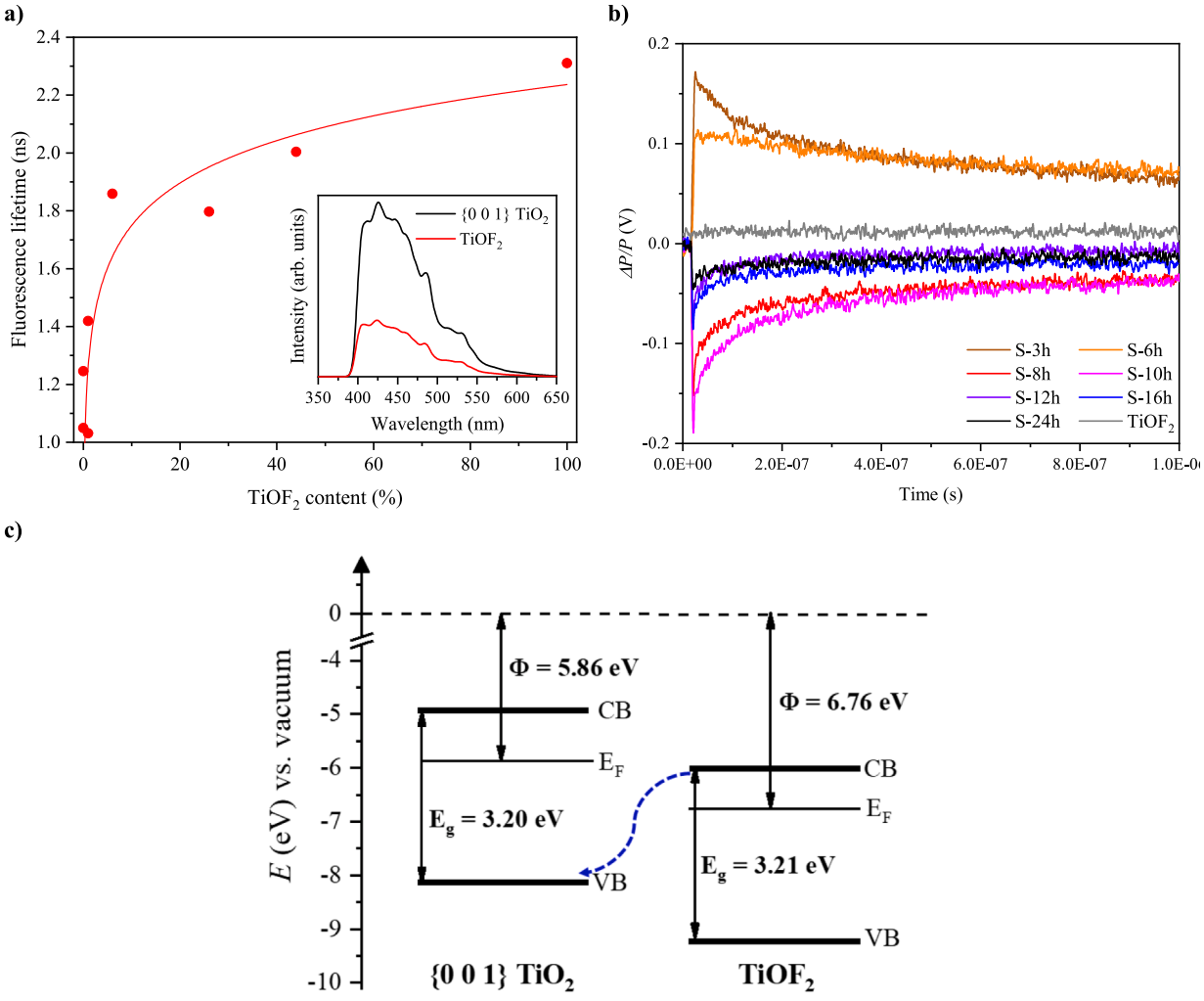

Fig. 9. a) Fluorescence lifetime for the different $TiO_2/TiOF_2$ samples *vs.* the $TiOF_2$ phase content. The solid line is a guide to the eye only; Inset shows the PL spectra of pure compounds at λ_{exc} = 320 nm, b) TRMC signal after excitation at λ = 360 nm for pure {0 0 1} anatase, $TiOF_2$ and $TiO_2/TiOF_2$ photocatalysts, c) Proposed mechanism of charge carriers separation in illuminated $TiO_2/TiOF_2$ based on lifetime measurements and DFT calculations; blue arrow shows the recombination process.

existing within its structure. In this regard, it seems reasonable that small amounts of $TiOF_2$ in the heterojunction can effectively withdraw both charge carriers from the composite structure, leading to boosted photocatalytic activity.

Considering the band structures of these two semiconductors, there are two possible charge carrier transfer pathways in the photocatalytic systems, that is, a traditional type-II heterojunction or a direct Z-scheme system. Therefore, DFT calculations were combined with fluorescence spectra to indicate the type of heterojunction between titanium oxyfluoride and {0 0 1} anatase. This time-resolved spectroscopy technique is supposed to be appropriate for heterojunction classification, as it provides insights into the evolution dynamics of photogenerated charge carriers within the heterojunction [49]. Fig. 9a shows the average fluorescence lifetimes obtained from exponential decay fittings of the fluorescence delay times measured for the different samples. An example of experimental and fitted exponential decay curves is presented in Fig. S12 in Supplementary Materials. Considering the single-phase compounds, $TiOF_2$ shows a remarkably longer fluorescence lifetime than TiO_2, which can be related to longer-lived electron-hole pairs. The composites show intermediate fluorescence lifetime values that reasonably follow an asymptotic trend with increasing $TiOF_2$ content. However, pure TiO_2 exhibited significantly higher fluorescence intensity than $TiOF_2$ (inset in Fig. 9a), so the determined fluorescence lifetimes in the composites originate from the anatase phase. Based on the presented trend, it can be noticed that $< \tau >$ increases for {0 0 1} TiO_2 when coupled to $TiOF_2$. In this system longer fluorescence lifetime, associated with higher number of photogenerated electrons, can be achieved when electrons from the CB of $TiOF_2$ recombine with holes from the VB of TiO_2. In the case of type-II heterojunction, electron flow should be into CB of $TiOF_2$, resulting in lower fluorescence intensity and lifetime. Therefore, according to the relative band positions obtained from DFT calculations, we suggest a Z-scheme heterojunction in {0 0 1} TiO_2/$TiOF_2$. This proposed heterojunction type aligns with the literature, where it has been studied using different techniques [50].

The TRMC measurements are presented in Fig. 9b. It can be observed that $TiOF_2$ itself does not show any signal, therefore this compound is supposed not to be photocatalytically active. All the compounds containing TiO_2 present a clear, typical high signal with well-defined decay. However, it can be noted that both S-3 h and S-6 h samples present a positive A sensitivity factor, whereas the others show signals with negative A factors. Therefore, it is not possible to compare I_{max} values of samples with opposite A factors. These differences in A factors for these series can be explained by significant variations in the microstructures. Composite structures consisting of two heterogeneous phases are always associated with important A factors variations. The structural analysis confirms this assumption – S-3 h and S-6 h are the only ones containing $TiOF_2$ in a significant amount with particular heterojunction structuration. The other photocatalysts with a low $TiOF_2$ content possess a similar behaviour to that of pure TiO_2 (S-16 h and S-24 h). However, in the range of synthesis time from 8 h to 24 h, it is possible to fully compare the TRMC signals. In this case, S-8 h and S-10 h exhibit the highest I_{max} values and slower decays, indicating a high number of charge carriers available for driving the surface redox reactions and the photocatalytic process.

Based on DFT calculations, VB-XPS spectroscopy and band gap measurements, we propose the band position of {0 0 1} TiO_2/$TiOF_2$ composite in relation to vacuum. Based on fluorescence lifetime measurements, the mechanism of electron and hole transport is suggested (Fig. 9c). This mechanism of charge carrier transfer is suitable for photocatalytic reactions because a Z-scheme photocatalyst has simultaneously a strong redox ability for driving photocatalytic reactions and spatially separated reductive and oxidative active sites. In the case of a type-II heterojunction, the advantage of charge carrier separation is at the expense of the redox abilities of charge carriers, which may weaken some specific surface redox reactions [51].

On the other hand, bulk $TiOF_2$ shows minimal photocatalytic activity in both oxidation and reduction processes. However, the low photoreactivity of a material does not preclude its efficient role in a heterojunction, as a material can produce electrons and holes under suitable irradiation while exhibiting minimal standalone photocatalytic activity. For example, Liang *et al.* reported the superior photocatalytic activity of Ag_2S/Cu_2O due to formation of Z-scheme heterojunction, although both pristine materials exhibited poor photocatalytic performance [52]. Although no signal was detected for pristine $TiOF_2$ in TRMC measurements, the calculated electron density distribution map revealed that its electronic structure significantly differs when used incorporated into the heterojunction compared to its standalone form. Due to this effect, comparing photocatalytic performance of $TiOF_2$ in the composite with its pristine form is challenging.

2.5. *Stability and reusability tests of the optimum TiO_2/$TiOF_2$ photocatalyst*

Reusability tests are of prime importance as leaching of fluorine ions from the {0 0 1} TiO_2/$TiOF_2$ photocatalysts can occur, whether it might come directly from the $TiOF_2$ phase or residual ions resulting from the HF-assisted solvothermal synthesis that forms the {0 0 1} TiO_2 facets. Using the most efficient S-8 h binary photocatalyst and the degradation of MCL under UV–vis irradiation, Fig. 10 shows the ability of the TiO_2/$TiOF_2$ system to be reused for five consecutive test cycles. The photocatalytic activity remained stable upon the first three cycles, with an average apparent kinetic rate constant k_{MCL} of 0.044 ± 0.002 min^{-1}. XRD patterns of the fresh and used photocatalysts showed that the {0 0 1} TiO_2/$TiOF_2$ photocatalysts undergo minor structural changes (Fig. S14 in Supplementary Materials) with similar crystallite size (14 nm), while XPS measurements evidenced an increase in the Ti/F surface ratio (Fig. S15 in Supplementary Materials) and a slight decrease in the Ti^{4+}–F contribution. The lower Ti^{4+}–F contribution than in the fresh sample and the slight increase in the Ti/F surface ratio were assigned to fluorine leaching, as confirmed by the ion chromatography (IC) analysis of the post-process water (Fig. S16 in Supplementary Materials). IC showed the presence of both F^- released by the photocatalyst, and Cl^- which originates from MCL mineralisation. The experimental Cl^- concentration was close to the theoretical value, which also confirmed the high efficiency of MCL dechlorination over three consecutive cycles. The slight decrease in the photocatalytic activity can be observed in fourth (0.0395 min^{-1}) and fifth cycle (0.0391 min^{-1}). Therefore, it is worth highlighting that although changes in the structure and surface, the photocatalytic activity is still high, so that the {0 0 1} TiO_2/$TiOF_2$ photocatalyst can be reused in water treatment.

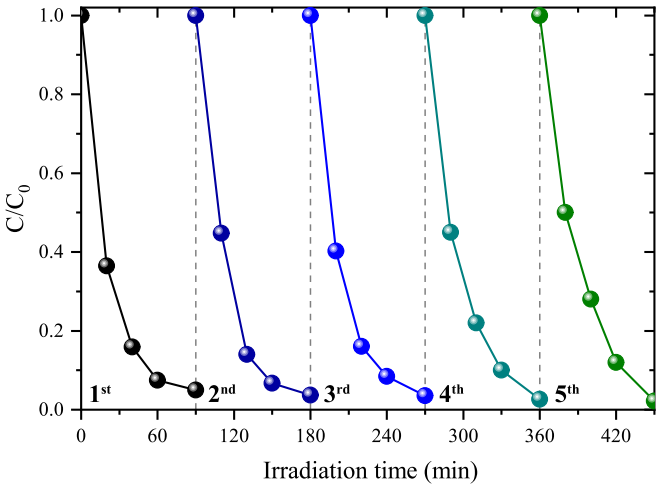

Fig. 10. Reusability tests of the MCL photocatalytic degradation on the S-8 h {0 0 1} TiO_2/$TiOF_2$ under UV–Vis light.

3. Conclusions

In the present work, the potential of {0 0 1} TiO_2/$TiOF_2$ heterojunction semiconductor photocatalysts was investigated for photocatalytic CECs oxidation and •OH generation. The combination of the $TiOF_2$ phase with highly energetic {0 0 1} crystal facets of anatase strongly enhanced both the degradation and the mineralisation of the organic pollutants. TRMC confirmed that the most photoactive samples (S-8 h and S-10 h) exhibited the highest number of charge carriers available for driving the surface redox reactions. Time-resolved fluorescence spectra revealed that charge carriers' lifetimes were prolonged when $TiOF_2$ was present in the final photocatalyst. DFT calculations and valence-band XPS spectra showed the favourable band position between both (0 0 1) TiO_2 and (1 0 0) $TiOF_2$ semiconductor phases, facilitating efficient migration and separation of photogenerated electron-hole pairs.

The $TiOF_2$ content in the binary photocatalyst, controlled by tuning the duration of the solvothermal synthesis, was a crucial factor which affected the photocatalytic performance. Regardless of the pollutant to degradation, the apparent kinetic rate constants for degradation as well as the TOC reduction efficiency feature a volcano-type behavior with increasing the $TiOF_2$ content. The highest performances were obtained on binary {0 0 1} TiO_2/$TiOF_2$ heterojunction photocatalysts with a low content of the $TiOF_2$ phase in the range 1.5–6 %, corresponding to synthesis durations of 8 h–12 h. These experimental results align well with DFT calculations which revealed a high potential barrier for $TiOF_2$ which is responsible for impeded electron migration. Therefore, efficient charge separation is achievable only when $TiOF_2$ forms thin structures at the (0 0 1) TiO_2 surface. Finally, reusability tests demonstrated high MCL degradation efficiency over five consecutive test cycles, despite minor structural changes.

The present study provides information about novel composition-controlled $TiOF_2$-based photocatalysts with improved charge carrier dynamics, as a key-factor for enhancing the degradation and mineralisation of a span of contaminants of emerging concern with varied chemical functions.

CRediT authorship contribution statement

Marta Kowalkińska: Writing – review & editing, Writing – original draft, Methodology, Investigation, Formal analysis, Conceptualization. **Nicolas Keller:** Writing – review & editing, Supervision, Methodology, Investigation, Formal analysis, Conceptualization. **Fernando Fresno:** Writing – review & editing, Investigation, Formal analysis. **Christophe Colbeau-Justin:** Investigation. **Anna Zielińska-Jurek:** Writing – review & editing, Validation, Supervision, Resources, Project administration, Methodology, Funding acquisition, Conceptualization.

Declaration of competing interest

The authors declare that they have no known competing financial interests or personal relationships that could have appeared to influence the work reported in this paper.

Acknowledgements

The research was financially supported by the Polish National Science Centre, grant no. UMO-2021/43/B/ST5/02983. The authors acknowledge the MEB-CRO platform in Strasbourg and T. Dintzer for SEM observations. V. Papaefthymiou (ICPEES, Strasbourg) is acknowledged for performing XPS characterisation. D. Ihiawakrim (IPCMS, Strasbourg) is thanked for performing TEM characterisation.

Appendix A. Supplementary data

Supplementary data to this article can be found online at https://doi.org/10.1016/j.apsusc.2025.162893.

Data availability

Data will be made available on request.

References

[1] European Environmental Agency, Chapter 10: chemical pollution, in: The European Environment-State and Outlook 2020. Knowledge for Transition to a Sustainable Europe, 2020, pp. 230–251, https://doi.org/10.2800/96749.
[2] V. Augugliaro, M. Bellardita, V. Loddo, G. Palmisano, L. Palmisano, S. Yurdakal, Overview on oxidation mechanisms of organic compounds by TiO_2 in heterogeneous photocatalysis, J. Photochem. Photobiol. C Photochem. Rev. 13 (2012) 224–245, https://doi.org/10.1016/j.jphotochemrev.2012.04.003.
[3] P. Garcia-Muñoz, F. Fresno, J. Ivanez, D. Robert, N. Keller, Activity enhancement pathways in $LaFeO_3$@TiO_2 heterojunction photocatalysts for visible and solar light driven degradation of myclobutanil pesticide in water, J. Hazard. Mater. 400 (2020) 123099, https://doi.org/10.1016/j.jhazmat.2020.123099.
[4] A. Habibi-Yangjeh, K. Pournemati, Z. Ahmadi, A. Khataee, Decoration of carbon dots on oxygen-vacancy-enriched s-scheme TiO_2 quantum Dots/TiO_2 oxygen vacancies photocatalysts: impressive quantum-dot-sized photocatalysts for remediation of antibiotics, bacteria, and dyes, Langmuir 40 (2024) 8503–8519, https://doi.org/10.1021/acs.langmuir.4c00060.
[5] K. Pournemati, A. Habibi-Yangjeh, S.R. Pouran, A. Khataee, Fabrication of TiO_2/CeO_2/$CeFeO_3$ tandem n-n heterojunction nanocomposites for visible-light-triggered photocatalytic degradation of tetracycline and colored effluents, Ceram. Int. 48 (2022) 22393–22402, https://doi.org/10.1016/j.ceramint.2022.04.241.
[6] A. Zielińska-Jurek, Z. Wei, M. Janczarek, I. Wysocka, Size - controlled synthesis of Pt particles on TiO_2 surface : physicochemical characteristic and photocatalytic activity, Catalysts 9 (2019) 1–18, https://doi.org/10.3390/catal9110940.
[7] F. Fang, Y. Liu, X. Sun, C. Fu, Y. Prakash Bhoi, W. Xiong, W. Huang, TiO_2 Facet-dependent reconstruction and photocatalysis of CuO_x/TiO_2 photocatalysts in CO_2 photoreduction, Appl. Surf. Sci. 564 (2021) 150407, https://doi.org/10.1016/j.apsusc.2021.150407.
[8] Y. Chen, L. Soler, C. Cazorla, N.G. Bastús, V.F. Puntes, J. Llorca, Facet-engineered TiO_2 drives photocatalytic activity and stability of supported noble metal clusters during H_2 evolution, Nat. Commun. 14 (2023) 6165, https://doi.org/10.1038/s41467-023-41976-2.
[9] S. Dudziak, M. Kowalkińska, A. Zielińska-Jurek, Chapter 3: crystal facet engineering of TiO_2 from theory to application, in: Updates on Titanium Dioxide, IntechOpen, 2023, https://doi.org/10.5772/intechopen.104130.
[10] H.G. Yang, C.H. Sun, S.Z. Qiao, J. Zou, G. Liu, S.C. Smith, H.M. Cheng, G.Q. Lu, Anatase TiO_2 single crystals with a large percentage of reactive facets, Nature 453 (2008) 638–641, https://doi.org/10.1038/nature06964.
[11] X. Han, Q. Kuang, M. Jin, Z. Xie, L. Zheng, Synthesis of titania nanosheets with a high percentage of exposed (001) facets and related photocatalytic properties, J. Am. Chem. Soc. 131 (2009) 3152–3153, https://doi.org/10.1021/ja8092373.
[12] J. Yu, J. Low, W. Xiao, P. Zhou, M. Jaroniec, Enhanced photocatalytic CO2-reduction activity of anatase TiO2 by co-exposed 001 and 101 facets, J. Am. Chem. Soc. 136 (2014) 8839–8842, https://doi.org/10.1021/ja5044787.
[13] S. Dudziak, M. Kowalkińska, J. Karczewski, M. Pisarek, K. Siuzdak, A. Kubiak, K. Siwińska-Ciesielczyk, A. Zielińska-Jurek, Solvothermal growth of 0 0 1 exposed anatase nanosheets and their ability to mineralize organic pollutants. The effect of alcohol type and content on the nucleation and growth of TiO2 nanostructures, Appl. Surf. Sci. 563 (2021) 150360, https://doi.org/10.1016/j.apsusc.2021.150360.
[14] M. Kowalkińska, S. Dudziak, J. Karczewski, J. Ryl, G. Trykowski, A. Zielińska-Jurek, Facet effect of TiO_2 nanostructures from $TiOF_2$ and their photocatalytic activity, Chem. Eng. J. 404 (2021) 126493, https://doi.org/10.1016/j.cej.2020.126493.
[15] J. Wang, F. Cao, Z. Bian, M.K.H. Leung, H. Li, Ultrafine single-crystal $TiOF_2$ nanocubes with mesoporous structure, high activity and durability in visible light driven photocatalysis, Nanoscale 6 (2014) 897–902, https://doi.org/10.1039/c3nr04489k.
[16] C.Z. Wen, Q.H. Hu, Y.N. Guo, X.Q. Gong, S.Z. Qiao, H.G. Yang, From titanium oxydifluoride ($TiOF_2$) to titania (TiO_2): phase transition and non-metal doping with enhanced photocatalytic hydrogen (H_2) evolution properties, Chem. Comm. 47 (2011) 6138–6140, https://doi.org/10.1039/c1cc10851d.
[17] L. Chen, L. Shen, P. Nie, X. Zhang, H. Li, Facile hydrothermal synthesis of single crystalline $TiOF_2$ nanocubes and their phase transitions to TiO_2 hollow nanocages as anode materials for lithium-ion battery, Electrochim. Acta 62 (2012) 408–415, https://doi.org/10.1016/j.electacta.2011.12.058.
[18] K. Lv, J. Yu, L. Cui, S. Chen, M. Li, Preparation of thermally stable anatase TiO_2 photocatalyst from $TiOF_2$ precursor and its photocatalytic activity, J. Alloys Compd. 509 (2011) 4557–4562, https://doi.org/10.1016/j.jallcom.2011.01.103.

[19] Z. Wang, K. Lv, G. Wang, K. Deng, D. Tang, Study on the shape control and photocatalytic activity of high-energy anatase titania, Appl. Catal. B 100 (2010) 378–385, https://doi.org/10.1016/j.apcatb.2010.08.014.

[20] L. Wang, J. Liu, Y. Min, K. Zhang, Nontopological transformation of hierarchical TiO_2 by self-regulated etching and capping roles of F^- for photocatalytic H_2 evolution, Appl. Surf. Sci. 473 (2019) 738–745, https://doi.org/10.1016/j.apsusc.2018.12.077.

[21] M. Kowalkińska, K. Sikora, M. Łapiński, J. Karczewski, A. Zielińska-Jurek, Non-toxic fluorine-doped TiO_2 nanocrystals from $TiOF_2$ for facet-dependent naproxen degradation, Catal. Today 415 (2022) 113959, https://doi.org/10.1016/j.cattod.2022.11.020.

[22] Y. Liu, Z. Ma, $TiOF_2$/g-C_3N_4 composite for visible-light driven photocatalysis, Colloids Surf. A. Physicochem. Eng. Asp. 618 (2021) 126471, https://doi.org/10.1016/j.colsurfa.2021.126471.

[23] P. Dong, E. Cui, G. Hou, R. Guan, Q. Zhang, Synthesis and photocatalytic activity of Ag_3PO_4/$TiOF_2$ composites with enhanced stability, Mater. Lett. 143 (2015) 20–23, https://doi.org/10.1016/j.matlet.2014.12.063.

[24] Z. Wang, K. Yu, Y. Feng, R. Qi, J. Ren, Z. Zhu, Stabilizing $Ti_3C_2T_x$-MXenes with $TiOF_2$ nanospheres intercalation to improve hydrogen evolution reaction and humidity-sensing performance, Appl. Surf. Sci. 496 (2019) 143729, https://doi.org/10.1016/j.apsusc.2019.143729.

[25] X. Ding, Z. Hong, Y. Wang, R. Lai, M. Wei, Synthesis of square-like anatase TiO_2 nanocrystals based on $TiOF_2$ quantum dots, J. Alloys Compd. 550 (2013) 475–478, https://doi.org/10.1016/j.jallcom.2012.10.049.

[26] Z. Liu, X. Liu, Q. Lu, Q. Wang, Z. Ma, $TiOF_2$/TiO_2 composite nanosheets: effect of hydrothermal synthesis temperature on physicochemical properties and photocatalytic activity, J. Taiwan Inst. Chem. Eng. 96 (2019) 214–222, https://doi.org/10.1016/j.jtice:2018.11.013.

[27] S. Dudziak, Z. Bielan, P. Kubica, A. Zielinska-Jurek, Optimization of carbamazepine photodegradation on defective TiO_2-based magnetic photocatalyst, J. Environ. Chem. Eng. 9 (2021) 105782, https://doi.org/10.1016/j.jece:2021.105782.

[28] E. Donner, T. Kosjek, S. Qualmann, K.O. Kusk, E. Heath, D.M. Revitt, A. Ledin, H. R. Andersen, Ecotoxicity of carbamazepine and its UV photolysis transformation products, Sci. Total Environ. 443 (2013) 870–876, https://doi.org/10.1016/j.scitotenv.2012.11.059.

[29] J.M. Monteagudo, A. Durán, R. González, A.J. Expósito, In situ chemical oxidation of carbamazepine solutions using persulfate simultaneously activated by heat energy, UV light, Fe^{2+} ions, and H_2O_2, Appl. Catal. B 176–177 (2015) 120–129, https://doi.org/10.1016/j.apcatb.2015.03.055.

[30] P. Garcia-Muñoz, W. Dachtler, B. Altmayer, R. Schulz, D. Robert, F. Seitz, R. Rosenfeldt, N. Keller, Reaction pathways, kinetics and toxicity assessment during the photocatalytic degradation of glyphosate and myclobutanil pesticides: influence of the aqueous matrix, Chem. Eng. J. 384 (2020) 123315, https://doi.org/10.1016/j.cej.2019.123315.

[31] C. Hou, H. Liu, F.B. Mohammad, Preparation of ordered mesoporous F–$H_2Ti_3O_7$ nanosheets using orthorhombic $HTiOF_3$ as a precursor and their highly efficient degradation of tetracycline hydrochloride under simulated sunlight, J. Solid State Chem. 300 (2021) 122288, https://doi.org/10.1016/j.jssc.2021.122288.

[32] X. Han, Q. Kuang, M. Jin, Z. Xie, L. Zheng, Synthesis of titania nanosheets with a high percentage of exposed (001) facets, J. Am. Chem. Soc. 131 (2009) 3152–3153, https://doi.org/10.1021/ja8092373.

[33] H.G. Yang, G. Liu, S.Z. Qiao, C.H. Sun, Y.G. Jin, S.C. Smith, J. Zou, H.M. Cheng, G. Q. Lu, Solvothermal synthesis and photoreactivity of anatase TiO2 nanosheets with dominant 001 facets, J. Am. Chem. Soc. 131 (2009) 4078–4083, https://doi.org/10.1021/ja808790p.

[34] Z. Huang, Z. Wang, K. Lv, Y. Zheng, K. Deng, Transformation of TiOF2 cube to a hollow nanobox assembly from anatase TiO2 nanosheets with exposed 001 facets via solvothermal strategy, ACS Appl. Mater. Interfaces 5 (2013) 8663–8669, https://doi.org/10.1021/am4023048.

[35] R. Ragsdale, B.B. Stewart, Fluorine-19 nuclear magnetic resonance study of some pentafluorotitanate complexes, Inorg. Chem. 2 (1963) 1002–1004, https://doi.org/10.1021/ic50027a031.

[36] Z. Lai, F. Peng, Y. Wang, H. Wang, H. Yu, P. Liu, H. Zhao, Low temperature solvothermal synthesis of anatase TiO2 single crystals with wholly 100 and 001 faceted surfaces, J. Mater. Chem. 22 (2012) 23906–23912, https://doi.org/10.1039/c2jm34880b.

[37] Q. Cheng, Y.J. Yuan, R. Tang, Q.Y. Liu, L. Bao, P. Wang, J. Zhong, Z. Zhao, Z.T. Yu, Z. Zou, Rapid hydroxyl radical generation on (001)-facet-exposed ultrathin anatase TiO_2 nanosheets for enhanced photocatalytic lignocellulose-to-H_2 conversion, ACS Catal. 12 (2022) 2118–2125, https://doi.org/10.1021/acscatal.1c05713.

[38] X. Zhao, G. Wei, J. Liu, Z. Wang, C. An, J. Zhang, Synthesis of heterostructured Pd@TiO_2/$TiOF_2$ nanohybrids with enhanced photocatalytic performance, Mater. Res. Bull. 80 (2016) 337–343, https://doi.org/10.1016/j.materresbull.2016.04.018.

[39] K. Kobayashi, M. Takashima, M. Takase, B. Ohtani, Mechanistic study on facet-dependent deposition of metal nanoparticles on decahedral-shaped anatase titania photocatalyst particles, Catalysts 8 (2018) 542, https://doi.org/10.3390/catal8110542.

[40] A. Zielińska-Jurek, Z. Bielan, S. Dudziak, I. Wolak, Z. Sobczak, T. Klimczuk, G. Nowaczyk, J. Hupka, Design and application of magnetic photocatalysts for water treatment The effect of particle charge on surface functionality, Catalysts 7 (2017) 360, https://doi.org/10.3390/catal7120360.

[41] H. Park, W. Choi, Effects of TiO_2 surface fluorination on photocatalytic reactions and photoelectrochemical behaviors, J. Phys. Chem. B 108 (2004) 4086–4093, https://doi.org/10.1021/jp036735i.

[42] A. Jain, S. Agarwal, S. Kumar, S. Yamaguchi, H. Miyaoka, Y. Kojima, T. Ichikawa, How does TiF_4 affect the decomposition of MgH_2 and its complex variants? - An XPS investigation, J. Mater. Chem. A 5 (2017) 15543–15551, https://doi.org/10.1039/c7ta03081a.

[43] G. Nansé, E. Papirer, P. Fioux, F. Moguet, A. Tressaud, Fluorination of carbon blacks: an X-ray photoelectron spectroscopy study: I. A literature review of XPS studies of fluorinated carbons. XPS investigation of some reference compounds, Carbon (1997) 175–194, https://doi.org/10.1016/S0008-6223(96)00095-4.

[44] S. Shian, K.H. Sandhage, Hexagonal and cubic $TiOF_2$, J. Appl. Crystallogr. 43 (2010) 757–761, https://doi.org/10.1107/S0021889810016730.

[45] S. Dudziak, M. Kowalkińska, J. Karczewski, M. Pisarek, J.D. Gouveia, J.R. B. Gomes, A. Zielińska-Jurek, Surface and trapping energies as predictors for the photocatalytic degradation of aromatic organic pollutants, J. Phys. Chem. C 126 (2022) 14859–14877, https://doi.org/10.1021/acs.jpcc.2c02775.

[46] Y. Nosaka, A.Y. Nosaka, Understanding hydroxyl radical (•OH) generation processes in photocatalysis, ACS Energy Lett. 1 (2016) 356–359, https://doi.org/10.1021/acsenergylett.6b00174.

[47] Y. Nosaka, A.Y. Nosaka, Generation and detection of reactive oxygen species in photocatalysis, Chem. Rev. 117 (2017) 11302–11336, https://doi.org/10.1021/acs.chemrev.7b00161.

[48] K. Cieślik, D. Wrana, M. Rogala, C. Rodenbücher, K. Szot, F. Krok, The effect of reduction and oxidation processes on the work function of metal oxide crystals: TiO_2(110) and $SrTiO_3$(001) case, Crystals 13 (2023) 1–17, https://doi.org/10.3390/cryst13071052.

[49] K. Spilarewicz, K. Mróz, M. Kobielusz, W. Macyk, When the fate of electrons matters — strategies for correct heterojunction classification in photocatalysis, Curr. Opin. Chem. Eng. 45 (2024) 101041, https://doi.org/10.1016/j.coche.2024.101041.

[50] Y. Chen, X. Wang, Z. Zeng, M. Lv, K. Wang, H. Wang, X. Tang, Towards molecular understanding of surface and interface catalytic engineering in TiO_2/$TiOF_2$ nanosheets photocatalytic antibacterial under visible light irradiation, J. Hazard. Mater. 465 (2024) 133429, https://doi.org/10.1016/j.jhazmat.2024.133429.

[51] Q. Xu, L. Zhang, J. Yu, S. Wageh, A.A. Al-Ghamdi, M. Jaroniec, Direct Z-scheme photocatalysts: principles, synthesis, and applications, Mater. Today 21 (2018) 1042–1063, https://doi.org/10.1016/j.mattod.2018.04.008.

[52] T.Y. Liang, S.J. Chan, A.S. Patra, P.L. Hsieh, Y.A. Chen, H.H. Ma, M.H. Huang, Inactive Cu_2O cubes become highly photocatalytically active with Ag_2S deposition, ACS Appl. Mater. Interfaces 13 (2021) 11515–11523, https://doi.org/10.1021/acsami.1c00342.